Hindawi
Geofluids
Volume 2022, Article ID 8013034, 13 pages
https://doi.org/10.1155/2022/8013034

WILEY | Hindawi

Research Article

Investigation of the Law of Natural Gas Phase Behavior during the Migration and Reservoir Formation

Longlong Li,[1] **Jiaren Ye**,[2] **Minqi Li**,[3] **and Lin Pan**[2]

[1]*Taiyuan University of Technology, Taiyuan, Shanxi 030024, China*
[2]*China University of Geosciences, Wuhan, Hubei 430074, China*
[3]*Exploration and Development Research Institute of Liaohe Oilfield, CNPC, Panjin, Liaoning 124010, China*

Correspondence should be addressed to Longlong Li; lilonglong@tyut.edu.cn

Received 25 February 2022; Revised 16 May 2022; Accepted 25 May 2022; Published 11 June 2022

Academic Editor: Yuxiang Zhang

It is of great significance to understand the phase regime of natural gas migration under high temperature and high pressure in the DF1-1 structure of Yinggehai Basin, South China Sea, to predict natural gas accumulation and evaluate resource reserves. However, the existing methane solubility models are not suitable for the higher temperature and pressure range required under current geological conditions. Through a self-designed experimental equipment with high precision, the solubility of CH_4 in deionized water can be measured in a wide range of temperatures (313.15-473.15 K) and pressures (5-200 MPa), and a reliable pressure-temperature-solubility segmented model is obtained by fitting. Using this model, we found that if the free-phase natural gas accumulated in the DF1-1 structural reservoir is completely dissolved in the water-soluble phase, the required formation water volume is much higher than the actual calculated formation water storage. Therefore, it can be inferred that the natural gas generated from the source rock of the DF13-1 structure mainly migrated and accumulated in the form of the free phase.

1. Introduction

Oil and gas exploration has developed to the deep layer of high temperature and high pressure (HTHP), but the migration phase of natural gas under high pressure remains quite complicated and unclear. CH_4 and water always exist as a symbiotic system under formation conditions. The phase balance and solubility of the CH_4-H_2O system under high temperature and high pressure are very important to understand the geological natural process of gas reservoir formation and gas reservoir development. The Yinggehai Basin in the South China Sea is a typical gas-bearing basin with HTHP. Some scholars believe that the migration phase of natural gas is mainly water soluble in this area [1–4]. The inference is that free natural gas is gradually separated from the formation water and then accumulated in the trap as the pressure decreases. Meanwhile, other researchers argue that natural gas migrates in both free and water-soluble phases. Therefore, predicting the solubility of natural gas (mainly CH_4) in water under high temperature and high pressure is the key to clarifying this problem.

With the in-depth study of the occurrence state and behavior characteristics of CH_4, many scholars have tested the solubility of CH_4 in deionized water within a certain range of temperature and pressure. The solubility of CH_4 under determined pressure (2~14.2 MPa) was firstly studied in 1931 by direct test of sampling [5]. Since then, scholars have made continuous breakthroughs in the field of medium and high pressure CH_4 solubility testing [6–16]. However, in the tests above, the test temperatures and pressures were mainly concentrated between 20 and 170°C and 0.1 and 70 MPa, respectively. In 2015, the solubility data of CH_4 in deionized water in the temperature range of 0~330°C and pressure range of 5~140 MPa were systematically tested by Raman spectroscopy which is an indirect test method of nonsampling [17]. Although the operation process was simplified, the effect of water vapor on the experimental results cannot be evaluated due to the small sample and the nonsampling test method adopted in this experiment. Nevertheless, the influence of the saturated vapor pressure on the solubility of CH_4 under high temperatures and pressures

was not negligible. Furthermore, solubility calculation models were presented based on phase equilibrium and incomplete experimental data [18–23].

The methods to study the solubility of CH_4 at high temperature and high pressure mainly include experimental tests and mathematical calculation models based on experimental test results (phase equilibrium equation), and experimental methods can be divided into the direct test method of sampling and the indirect test method of closed nonsampling. Fan et al. [24], Nighswander et al. [25], Messabeb et al. [26], and Qin et al. [27] used the direct sampling method to test the solubility of CH_4/CO_2 in pure water/formation water. After reaching the dissolution equilibrium, samples were taken, gas-liquid separation was performed, and gas-liquid volume was measured to calculate its solubility. This kind of measurement method is prone to deviation in the process of gas-liquid separation measurement, resulting in low accuracy of experimental results. Ou et al. [17] used the indirect test sampling method to test the solubility of CH_4/CO_2 in pure water/formation water. Its advantage is to reasonably avoid the measurement deviation of sampling and process of separation, but as a result, the test methods need to use existing data obtained by the sampling method to proofread the spectral characteristics; therefore, this method of test accuracy depends on the accuracy of the test results of the previous sampling method.

In order to solve the phase behavior of hydrocarbon gas accumulation and migration under the condition of HTHP, the solubility of the CH_4-H_2O was measured in this study over a wide range of temperatures and pressures: 313.15-473.15 K and 5-200 MPa (Figure 1). This test method eliminates the effect of saturated vapor pressure on solubility. On this basis, the CH_4-H_2O solubility model was established, the boundary conditions of the model parameters were clarified, and the DF13-1 structure natural gas migration phase state was predicted using the model. Based on the new test results, we can more accurately research the accumulation mechanism, migration phase state, and organic and inorganic theory of CH_4 formation from the ultradeep formation and evaluate the reserves of gas reservoir development.

2. Experimental Settings

2.1. Apparatus and Materials. As shown in Figure 1, the test instrument consisted of a gas-liquid injection metering system, a HTHP dissolution equilibrium vessel, a sampling system, a depressurization system, and a measurement system which is connected to a gas chromatograph (GC) for detection. The dissolution equilibrium container is located in a thermostat (273.15~573.15 K, ±0.1 K) and is connected with a constant speed and constant pressure pump (0~200 MPa, ±0.1 MPa). The temperature and pressure sensor (273.15 K/373.15 K, ±0.1 K/200 MPa, ±0.1%) is used to measure the temperature in the thermostat and the temperature and pressure in the dissolution equilibrium container, which are monitored through the control panel and recorded in the computer.

The dissolution equilibrium container is a cylindrical design with an internal effective volume of 600 mL, which can hold a large amount of fluid and provides enough space for phase balance. The constant-speed and constant-pressure pump is equipped with a high-precision displacement sensor (0~300 mm, ±0.01 mm) on its side wall, which is used to measure the position of the moving piston in the container to allow monitoring of the volume change of the fluid.

The fluid is injected into the intermediate container through a booster pump and then injected into the dissolution equilibrium container through a pressure-regulating valve and a mass flowmeter (up to 20,000 mL, ±2.0%). The injection port is located at the bottom of the dissolution equilibrium container. In the experiment, deionized water/formation water is firstly injected into the dissolution equilibrium container, and then, the gas is injected through the liquid to reach full mixing. Samplers are designed on the side wall and top of the dissolution equilibrium container. Each sampler has an internal volume of 0.1 mL for collecting both vapor and liquid samples at the same time. Because the sampled volume is relatively small, the constant temperature and pressure sampling will not affect the phase balance in the container. Then, rebalance is achieved through the constant temperature and pressure system, and the balanced sample is injected into the calibrated GC for concentration analysis. The detection ranges of CH_4 and H_2O in the GC are 0.001×10^{-5}~5×10^{-5} mol and 0.001~10 mg, respectively.

The CH_4 used in the experiment is bottled gas with a purity of 99.99% and an initial pressure of 10~12 MPa. Deionized water is used in all the experiments in which the concentrations of Cl^-, Ca^{2+}, and Mg^{2+} in this water are 0 mg/L, and the concentration of Na^+ and tolerable silicon is less than 0.01 mg/L.

2.2. Procedures. In this study, the test of the process includes system vacuum leak detection, rule pressurization, system injection of fluid, heating and pressurization of solution kettle, temperature and pressure balancing operation, holding sampling, solubility testing, and processing of experimental results.

Vacuum leak detection was performed before each experiment. After the system was connected, the whole system was vacuumed in order to detect leakage. If the high vacuum mode of each part of the reaction chamber, connecting pipelines, and other parts could be maintained for more than 20 minutes (the data displayed on the pressure gauges of each part remains unchanged), the airtightness of the connection of this system is considered as good.

After no leak is detected, the equipment was vacuumed again and the experiment started. H_2O was firstly injected into the container, followed by CH_4. The amount of CH_4 injection was measured and recorded with a mass flowmeter. Data from temperature, pressure, and displacement sensors were also used for CH_4 injection approval calculation. After the injection was completed, the temperature and pressure of the dissolution equilibrium container were adjusted to the experimental temperature and pressure by heating and pressurization. Once the temperature and pressure of the container were set, the system was designed to automatically maintain constant temperature and pressure and recorded

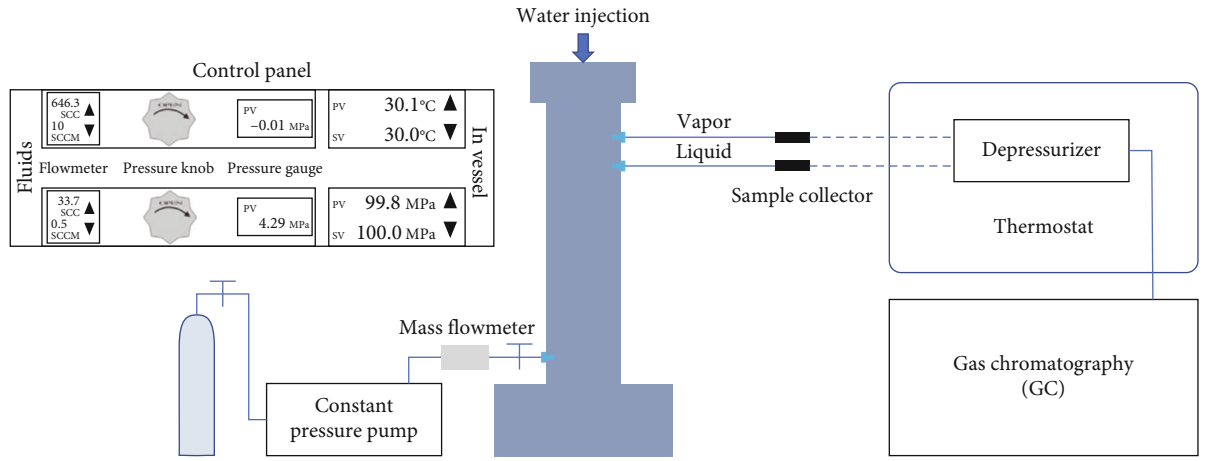

Figure 1: Schematic illustration of apparatus.

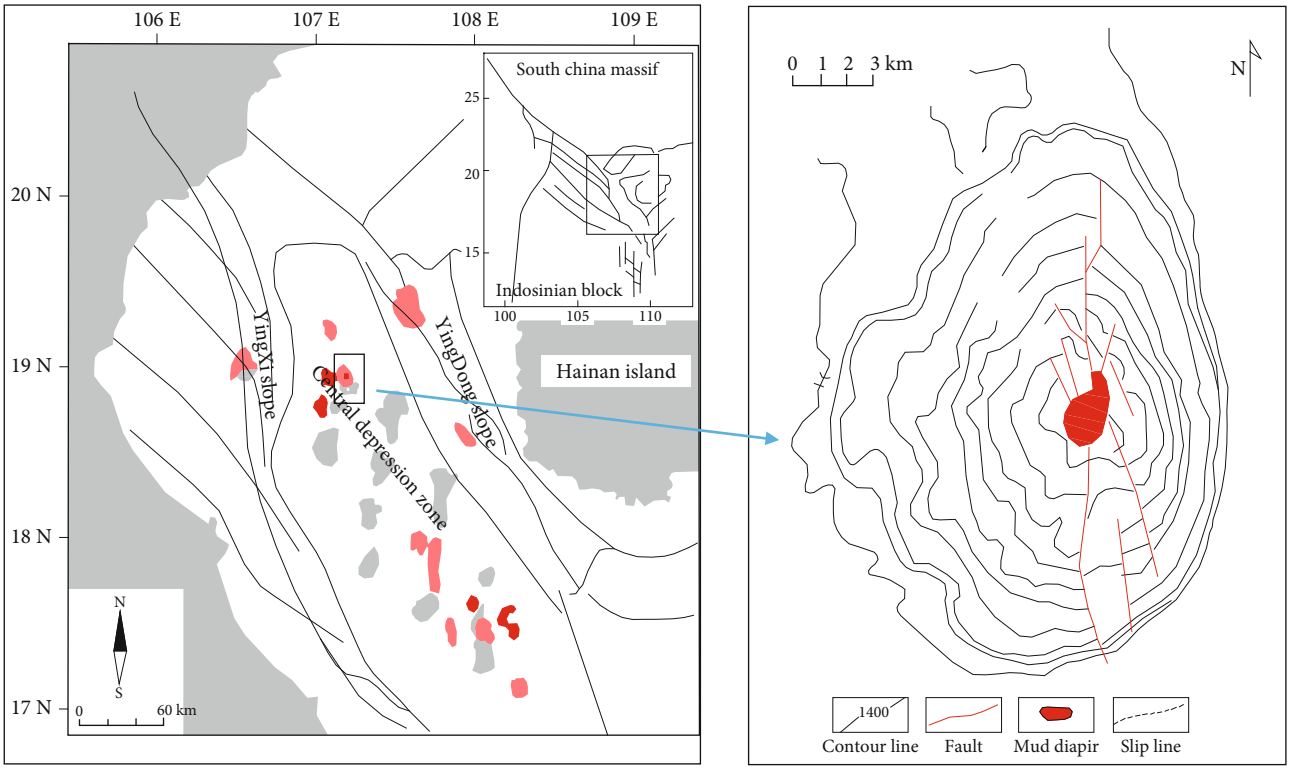

Figure 2: Location and tectonic map of DF1-1 (data from the China National Offshore Oil Corporation).

the temperature, pressure, and displacement sensor data every 5 minutes.

Dissolution equilibrium was reached after 6~24 h of constant temperature and pressure. The higher the temperature, the shorter the time required for dissolution equilibrium. Then, sampling was conducted after dissolution equilibrium to ensure that the phase state, temperature, and pressure of the fluid in the sampler were the same as those in the dissolution equilibrium container. The vapor sample was directly sent to the GC for fraction analysis after a rebalance treatment involving temperature elevation and pressure reduction. Finally, the solubility of CH_4 in water under the defined temperature and pressure conditions was calculated based on the composition of the vapor sample and the liquid sample (Equation (1)). The accuracy of solubility was confirmed by repeated sampling of the fluid in the dissolution equilibrium container at defined temperature and pressure.

$$m_{CH_4} = \frac{n_{CH_4}}{m_{H_2O}} \times 10^6, \quad (1)$$

in which, m_{CH_4} is the solubility of CH_4, mol/kg; n_{CH_4} is the amount of CH_4, mol; and m_{H_2O} is the mass of H_2O, mg.

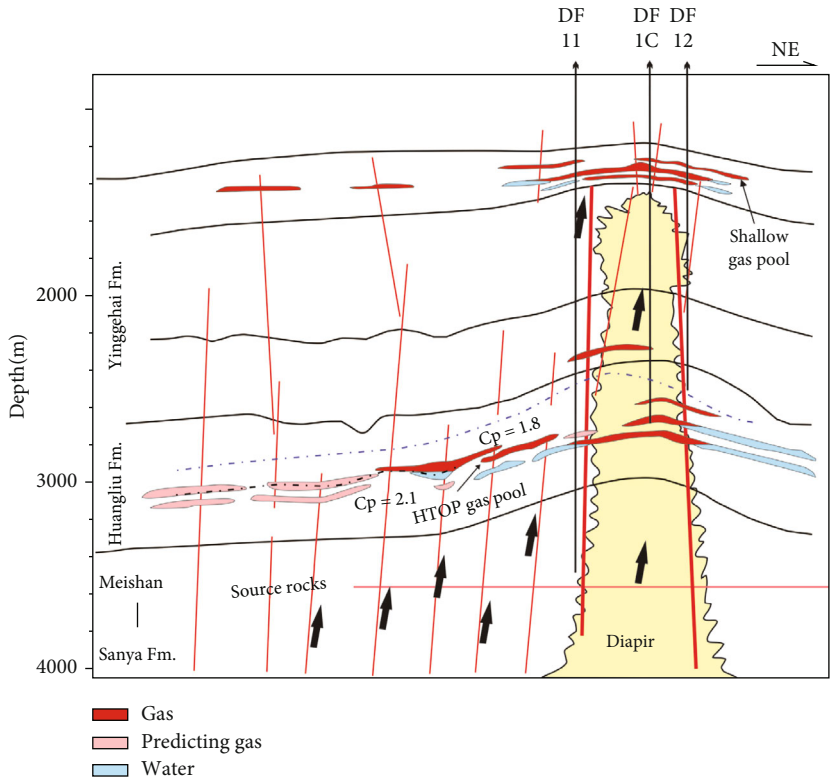

Figure 3: Gas location and tectonic section map of DF1-1.

Table 1: Calculated CH_4 solubility in H_2O (mCH_4, mol/kg).

P (MPa)	*T* (K)									
	313.15	333.15	353.15	363.15	373.15	393.15	413.15	433.15	453.15	473.15
5	0.0436	0.0392	0.0385	0.0383	0.0383	0.0387	0.0416	0.0457	0.0495	0.0541
10	0.0892	0.0713	0.0702	0.0787	0.0791	0.0798	0.0854	0.0953	0.1078	0.1256
15	0.1206	0.1012	0.0979	0.1061	0.1069	0.1123	0.1239	0.1396	0.1612	0.1911
20	0.1445	0.1273	0.1216	0.1204	0.1216	0.1382	0.1571	0.1786	0.2096	0.2506
30	0.1772	0.1592	0.1533	0.1541	0.1563	0.1735	0.1986	0.2348	0.2756	0.3455
40	0.2083	0.1881	0.1821	0.1832	0.1874	0.2086	0.2374	0.2881	0.3405	0.4194
50	0.2306	0.2125	0.2108	0.2123	0.2185	0.2427	0.2762	0.3414	0.4058	0.4933
60	0.2563	0.2379	0.2363	0.2368	0.2461	0.2677	0.3124	0.3918	0.4692	0.5463
70	0.2806	0.2623	0.2604	0.2608	0.2744	0.3011	0.3474	0.4232	0.5049	0.6026
80	0.3024	0.2855	0.2832	0.2838	0.3027	0.3331	0.3822	0.4546	0.5406	0.6573
90	0.3228	0.3045	0.3048	0.3159	0.3311	0.3609	0.4168	0.4861	0.5763	0.7103
100	0.3449	0.3222	0.3228	0.3247	0.3481	0.3807	0.4368	0.5071	0.6123	0.7479
110	0.3647	0.3398	0.3408	0.3425	0.3652	0.4005	0.4568	0.5281	0.6483	0.7855
120	0.3824	0.3564	0.3588	0.3653	0.3819	0.4203	0.4769	0.5489	0.6843	0.8231
130	0.3966	0.3775	0.3807	0.3866	0.4062	0.4481	0.5018	0.5887	0.7088	0.8543
140	0.4088	0.3956	0.3984	0.4049	0.4264	0.4719	0.5307	0.6218	0.7333	0.8845
150	0.4213	0.4117	0.4171	0.4232	0.4456	0.4957	0.5594	0.6549	0.7578	0.9146
160	0.4312	0.4288	0.4336	0.4426	0.4668	0.5196	0.5968	0.6853	0.7823	0.9437
170	0.4402	0.4399	0.4448	0.4543	0.4829	0.5368	0.614	0.7076	0.8103	0.9747
180	0.4486	0.447	0.452	0.462	0.495	0.5501	0.6272	0.7259	0.8342	1.0012
190	0.4565	0.4552	0.4592	0.4697	0.5064	0.5623	0.6405	0.7442	0.8582	1.0277
200	0.4624	0.4613	0.4664	0.4774	0.5192	0.5764	0.6536	0.7623	0.8821	1.0535

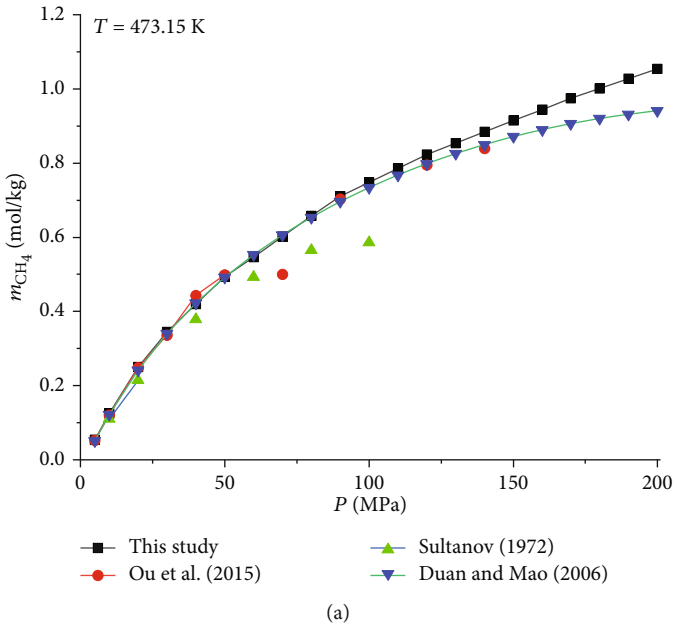

(a)

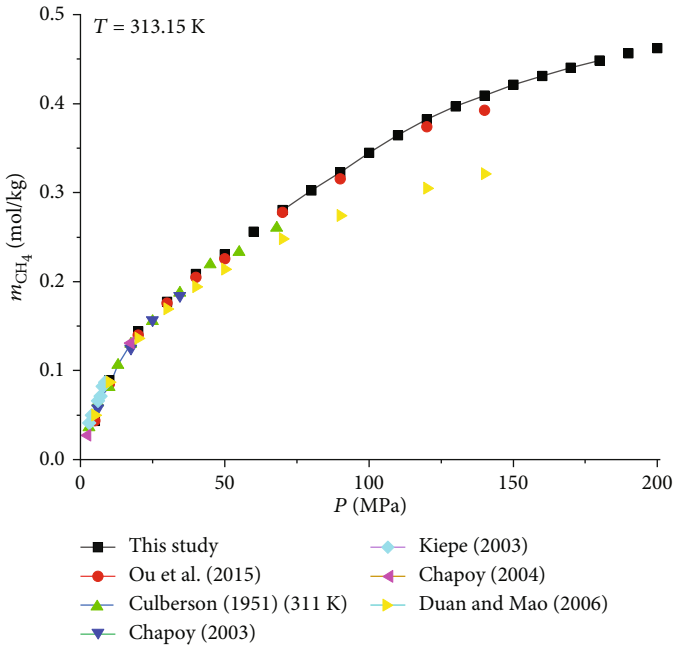

(b)

Figure 4: Continued.

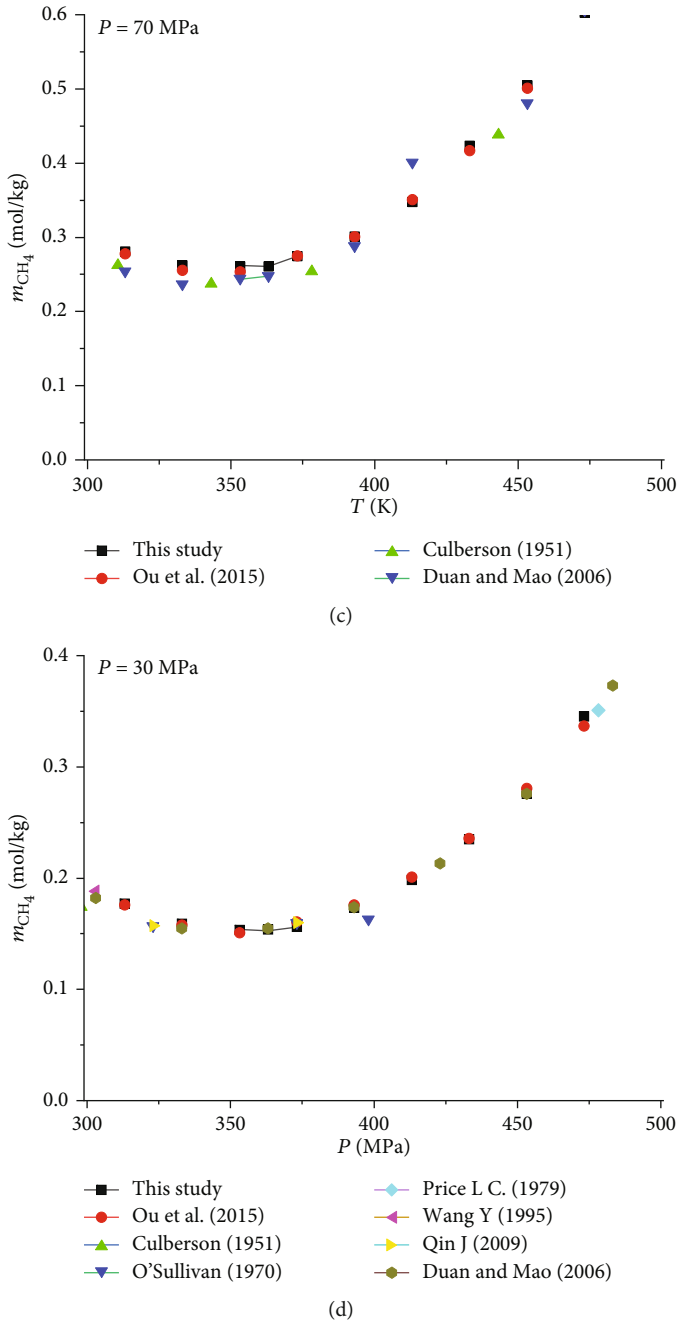

FIGURE 4: Representative diagram of m_{CH_4} at different conditions and the comparison with published data: (a) $T = 473.15$ K; (b) $T = 313.15$ K; (c) $P = 70$ MPa; (d) $P = 30$ MPa.

3. Geological Setting

Yinggehai Basin is located in the Yinggehai sea area between Hainan Island of China and Vietnam. The basin has an overall NNW-trending rhombic structure with an aspect ratio of about 2.5 : 1, and the sea area is 4.5×10^4 km^2. The basin is sandwiched between the extrusion-escape structure in the west and the subduction-drag structure in the east of the Paleo-South China Sea. Large, deep strike-slip faults such as the Honghe fault cut across the edge of the basin, with a unique characteristic of high geothermal gradient (4.6°C/100 m) and abnormally high-pressure gradient (1.0~2.1 MPa/100 m) [28, 29]. The sedimentary caprocks drilled in the basin mainly include the Lower Oligocene Yacheng Formation (E_3y), the Upper Oligocene Lingshui Formation (E_3l), the Lower Miocene Sanya Formation (N_1s), the Middle Miocene Meishan Formation (N_1m), the Upper Miocene Huangliu (N_1h), and the Yinggehai Formations (N_2y). After more than 30 years of exploration, a number of oil- and gas-bearing structures with commercial development value have been discovered in the basin (Figure 2).

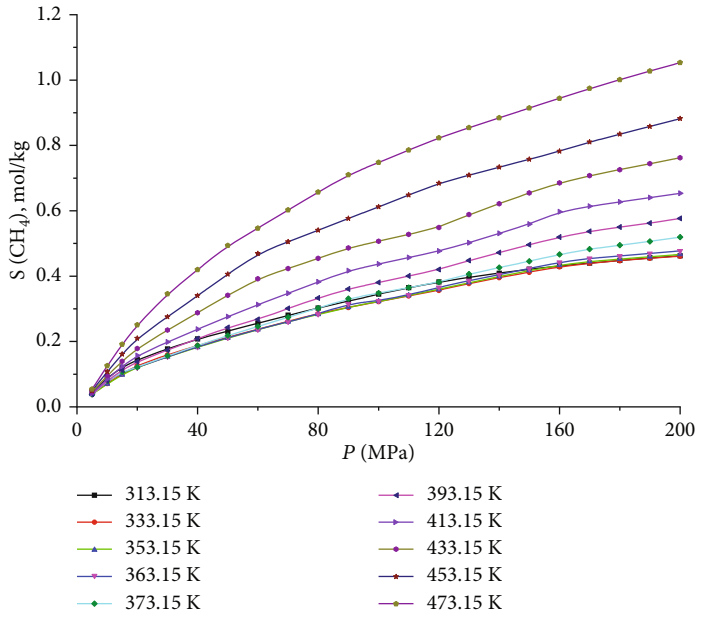

Figure 5: P-S-T curve of solubility in CH_4 pure water.

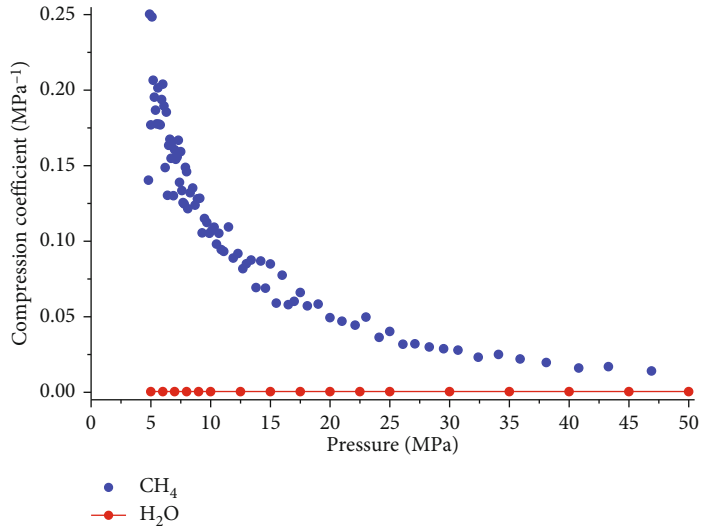

Figure 6: Comparison of compressibility between CH4 and water in 353.15 K.

The source rocks in the basin are the mid-high maturity level marine mudstones of the Lower Miocene Sanya and Middle Miocene Meishan Formations. It is characterized by high abundance of organic matter, partial humic type (II_2-III) as the main kerogen type, middle to high maturity stage, and strong gas generating ability. The discovered natural gas reservoirs in this basin are mainly distributed in sandstone reservoirs of the second member of the Yinggehai Formation and the first member of the Huangliu Formation. The reservoir lithology of the second member of the Yinggehai formation is mainly siltstone and argillaceous siltstone, with an average porosity of 20.6% and permeability 2.7~1000 mD. The reservoir lithology of the first member of the Huangliu Formation is mainly siltstone and fine sandstone. Its grain size is coarser than that of the Yinggehai Formation, with an average porosity of 13~19.8% and a permeability of 3.1~34.2 mD. The lithology of the first member of the Yinggehai Formation is mainly composed of a large set of mudstone with a small amount of gray siltstone and argillaceous siltstone. It acts as an excellent caprock widely distributed across the basin with a mean thickness of about 320 m.

The DF1-1 structure, located in the northwest of the central diapir belt of the basin, is a simple short-axis anticline of mud diapir origin and cut by arch-extensional faults (Figures 2 and 3 [30]). The structure strikes nearly north-south, steeply dipping in the east and gently dipping in the west, and has good inheritance. The trap area is up to

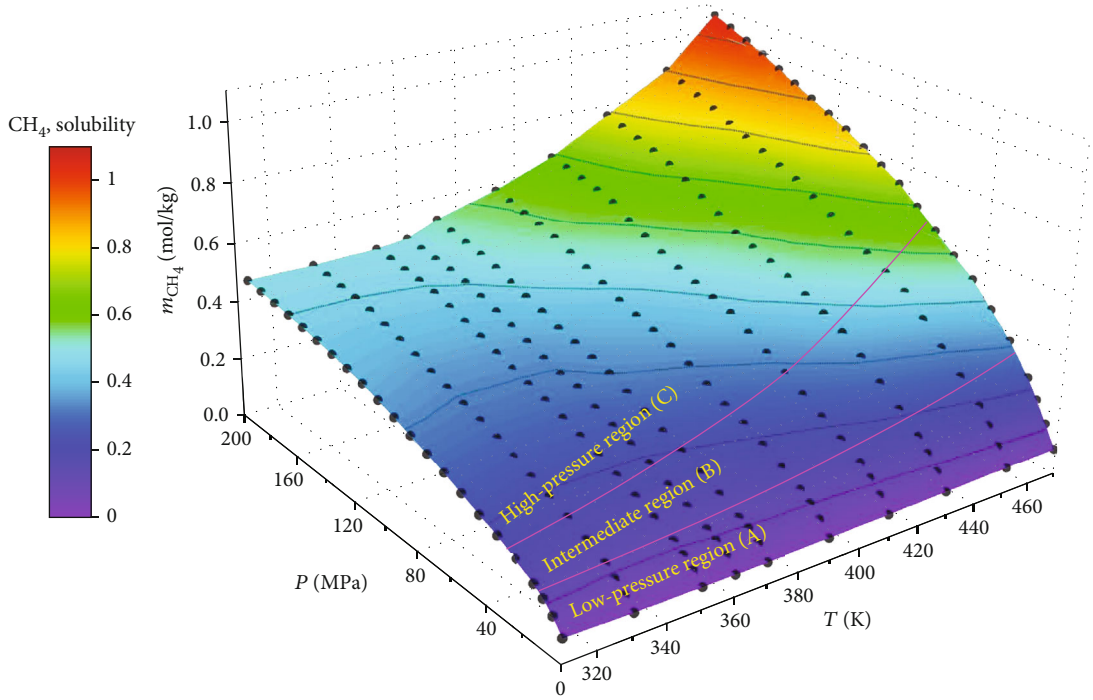

FIGURE 7: The m_{CH4} surface in three dimensions. The dots are experimental measurements in this work. The pink solid lines divide the surface into three regions: A, low-pressure region; B, intermediate region; and C, high-pressure region. The controlling effects of P and T are different in each region.

300 km^2 (Figure 2), and the natural gas is buried shallowly (1200 m-1600 m). According to results from exploration and development, DF1-1 is a dry gas reservoir, in which the main hydrocarbon in natural gas is CH_4, and the content of components above C_2 is relatively low (0.63%-2.61%). As of August 2008, the hydrocarbon gas reserves in the DF1-1 structure were 594.22×10^8 m^3 [31].

4. Results

4.1. Test Results and Reliability Analysis. The temperature and pressure ranges covered by this experiment are 313.15 K~473.15 K and 5 MPa~200 MPa, respectively, and 220 effective data points of the solubility of CH_4 in H_2O have been obtained in the experiment (Table 1).

According to the distribution of published experimental data, the data of solubility with pressure at 313.15 K and 473.15 K and the data of solubility with temperature under 30 MPa and 70 MPa were compared with the published results. Compared with the published results, the measurement of this work covers a wider range of temperature and pressure. In the region of low pressure $(P) < 60$ MPa and temperature $(T) < 373.15$ K, the test data of this experiment are in good agreement with the published data. However, the values are larger than previously published data at high pressures and temperatures since we have eliminated the effect of saturated vapor pressure in this work (Figure 4).

According to the P-S-T curve obtained from the solubility test of CH_4 in pure water (Figure 5), when the temperature is constant, the solubility of CH_4 in pure water increases gradually with the increase of pressure, showing a general trend of first fast and then slowing down. The solubility change of CH_4 in pure water is determined by phase equilibrium during the process of constant temperature and increasing pressure.

In the dissolved system of CH_4-H_2O, when pressure is increasing with constant temperature, the density of H_2O increases and the accommodating space of water decreases. However, the compressibility coefficient of CH_4 changes much more than that of H_2O in this process (Figure 6); in this result, more CH_4 can be accommodated in the smaller water molecular gap. On the macroscopic scale, the solubility of CH_4 in pure water increases unidirectionally with the increase of pressure.

With the increase of pressure, the compressibility coefficient of CH_4 gradually decreases; as a result, the solubility of CH_4 in pure water increases rapidly at first and then slowly under the condition of pressure increase and constant temperature. At higher temperature and pressure, the compressibility of CH_4 approaches to a constant value, which can be predicted that the solubility of CH_4 in pure water will not increase infinitely with increasing pressure.

4.2. The P-T-mCH_4 Model. The solubility of CH_4 in an aqueous solution is dependent on the equilibrium of the chemical potential of CH_4 in the liquid phase $(\mu^l_{CH_4})$ and the gas phase $(\mu^v_{CH_4})$. The potential can be expressed by the fugacity (f) in the gas phase and the activity (a) in the liquid phase:

$$\begin{aligned}\mu^v_{CH_4}(T,P,y) &= \mu^{v(0)}_{CH_4}(T) + RT\ln f_{CH_4}(T,P,y)\\ &= \mu^{v(0)}_{CH_4}(T) + RT\ln y_{CH_4}P + RT\ln \varphi_{CH_4}(T,P,y),\end{aligned} \quad (2)$$

Table 2: The polynomial models of CH_4 solubility in H_2O (m_{CH_4}, mol/kg).

Region	Boundary condition T (K)	Boundary condition P (MPa)	Fitting model	Coefficient (with 95% confidence bounds)	Goodness of fit (R^2)
A	313.15~473.15	$P < -0.000155T^2 + 0.1793T - 23.8842$	$m_{CH4} = a_1 + a_2P + a_3T + a_4P^2 + a_5PT$	$a_1 = 0.095$ $a_2 = -0.10014$ $a_3 = 0$ $a_4 = 0.0000214$ $a_5 = 0.00005922$	0.9461
B	313.15~473.15	$-0.000155T^2 + 0.1793T - 23.8842 \le P < -9.253 \times 10^{-7}T^3 + 0.001T^2 - 0.259T + 24.1000$	$m_{CH4} = a_1 + a_2P + a_3T + a_4P^2 + a_5PT + a_6T^2 + a_7P^2T + a_8PT^2 + a_9P^3$	$a_1 = 0.984$ $a_2 = 0.025$ $a_3 = -0.004$ $a_4 = 0.000018$ $a_5 = 0$ $a_6 = 0.000005231$ $a_7 = -0.0000004748$ $a_8 = 0.0000002818$ $a_9 = 0.0000001112$	0.9992
C	313.15~473.15	$P \ge -9.253 \times 10^{-7}T^3 + 0.001T^2 - 0.259T + 24.1000$	$m_{CH4} = a_1 + a_2P + a_3T + a_4P^2 + a_5PT + a_6T^2 + a_7P^2T + a_8PT^2 + a_9T^3$	$a_1 = 0.876$ $a_2 = 0.005$ $a_3 = 0.000009349$ $a_4 = -0.000004505$ $a_5 = -0.000002029$ $a_6 = -0.000001849$ $a_7 = -0.00000001237$ $a_8 = 0.00000003637$ $a_9 = 0.00000003419$	0.9997

where the gas constant R is 0.08314467 bar×L/(mol × K); y and y_{CH_4} are the mole fraction of CH_4 in the gas phase; and φ_{CH4} is the fugacity coefficient.

$$\begin{aligned}\mu^{l}_{CH_4}(T,P,m) &= \mu^{l(0)}_{CH_4}(T) + RT\ln a_{CH_4}(T,P,m)\\ &= \mu^{l(0)}_{CH_4}(T,P) + RT\ln m_{CH_4}\\ &\quad + RT\ln \gamma_{CH_4}(T,P,m),\end{aligned} \tag{3}$$

where m and m_{CH_4} denote the molarity of CH_4 in the liquid phase; γ_{CH_4} denotes the activity coefficient. In equilibrium, $\mu^{v}_{CH_4} = \mu^{l}_{CH_4}$; the equation can be written as

$$\begin{aligned}\ln\frac{y_{CH_4}P}{m_{CH_4}} &= \frac{\mu^{l(0)}_{CH_4}(T,P) - \mu^{v(0)}_{CH_4}(T)}{RT} - \ln\varphi_{CH_4}(T,P,y)\\ &\quad + \ln\gamma_{CH_4}(T,P,m).\end{aligned} \tag{4}$$

$\mu^{l}_{CH_4}$ and $\ln\varphi_{CH_4}$ are functions of T and P. Since our measurements cover a wide range of temperatures and pressures, we can create a surface showing CH_4 solubility varying with temperature and pressure, where P is the X axis, T is the Y axis, and CH_4 is the Z axis (Figure 7).

According to the law of CH_4 solubility changing with temperature and pressure, the surface is divided into three regions, and each region is fitted and modeled (Figure 7). The fitted boundary conditions for these regions are given in Table 2. In region A (low pressure region), m_{CH_4} is mainly a function of pressure, and m_{CH_4} has a low solubility (usually less than 0.2 mol/kg). In this region, m_{CH_4} increases with the increase of pressure and decreases with the increase of temperature, but the rate of change is very limited. In region B (middle pressure region), m_{CH_4} shows a general trend of increase with increasing pressure and temperature. In this region, pressure is the main controlling factor of m_{CH_4}, but its dependence on pressure is not as strong as that in region A. In region C (high pressure region), the effects of temperature and pressure on m_{CH4} are more complex than those in the other two regions. In this region, the effect of the temperature on m_{CH_4} is greater than that of the pressure. When $T < 363.15$ K, m_{CH_4} increases with increasing pressure and decreasing temperature and reaches a maximum value (0.4624 mol/kg) at a maximum pressure of 200 MPa and a minimum temperature of 313.15 K. When $T > 363.15$ K, m_{CH_4} increases with increased pressure and temperature and reaches a maximum value (1.0535 mol/kg) at 200 MPa and 473.15 K. The three polynomials obtained by curve fitting are in good agreement with the experimental data (Table 2).

5. Discussion

The existing drilling results reveal that the source rock burial depth of the Meishan Formation in the Yinggehai Basin is 3200~4700 m, and the source rock burial depth of the Sanya Formation is 4700~5500 m (the base of this formation was not penetrated). The formation temperature and pressure data at different depths were obtained using the literature data [32, 33] (Table 3).

Table 3: Paleotemperature and pressure data table of different depths in DF1-1 area (data from the China National Offshore Oil Corporation).

Depth (m)	T (K)	P (MPa)
1000	333.15	10.7
1200	347.15	12.9
1400	353.45	15
1600	362.85	17.2
2300	391.45	24.7
3000	421.25	39.2
3300	435.25	50.2
3500	444.55	60.1
4000	468.05	70
4500	492.15	81.6
5000	513.25	90.1
5500	535.85	100
6000	557.75	111.5

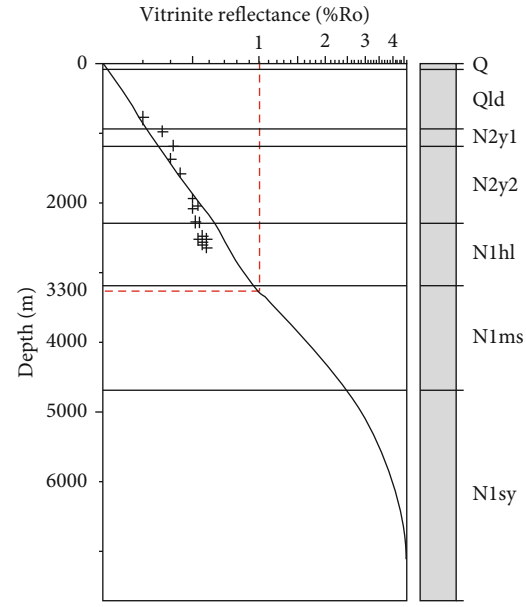

Figure 8: Vertical distribution of source rock maturity in DF1-1 (data from the China National Offshore Oil Corporation).

The relationship between vitrinite reflectance and depth is shown in Figure 8. In Figure 8, the legend on the right shows the corresponding relationship between stratigraphic sequence and formation depth of the DF1-1 structure, the cross-star represents the measured data, and the solid black line represents the fitting result, obviously. The red dotted line indicates the burial depth corresponding to 1% vitrinite reflectance. The source rock maturity simulation results show that the corresponding burial depth is about 3300 m when the source rock of the DF1-1 structure generates a

Table 4: Table of applicable conditions for DF1-1 regional hydrocarbon generation and accumulation solubility model.

	Formation temperature (K)	Boundary conditions of solubility model (P, MPa)	Formation pressure (MPa)	Using model types
The depth of hydrocarbon generation	435.25	<26.8	50.2	B area
		$26.8 \le P < 62.2$		
		≥62.2		
The depth of accumulation	353.45	<20.1	15	A area
		$20.1 \le P < 41.5$		
		≥41.5		

large amount of hydrocarbons (Ro = 1.0%). Existing research shows that the natural gas reservoirs in the DF1-1 structure are concentrated at the depth of 1200 m to 1600 m, with an average depth of 1400 m [33]. As shown in Table 3, for the DF1-1 structure, the temperature and pressure of the depth of large-scale hydrocarbon generation are 435.25 K and 50.2 MPa, respectively, and the temperature and pressure of the depth of large-scale accumulation are 353.45 K and 15 MPa, respectively.

When the hydrocarbon generation and accumulation temperature of the DF1-1 structure are introduced into the CH_4 solubility mathematical model, the boundary conditions can be obtained. Compared with the hydrocarbon generation and accumulation formation pressure (Table 4), it can be seen that in the depth of hydrocarbon generation, the formation pressure is between 26.8 and 62.2 MPa, which is suitable for zone B of the CH_4 solubility model; meanwhile, in the depth of accumulation, the formation pressure is lower than 20.1 MPa, so it is suitable for zone A of the CH_4 solubility model.

The temperature and pressure conditions of hydrocarbon generation and accumulation are introduced into the corresponding CH_4 solubility model (Table 2), and the solubility of CH_4 under the corresponding conditions is obtained: 0.3478 mol/kg for the hydrocarbon generation and 0.0979 mol/kg for accumulation. The research results show that under condition of the same temperature and pressure difference, the exsolution quantity of CH_4 is about 4% lower than the dissolved quantity, while the solubility of CH_4 in formation water is 2%~7% lower than that of deionized water [34], and the higher the temperature and pressure, the smaller the difference. Based on this, it is assumed that the DF1-1 structure is exsoluted, and being accumulated in a water-soluble phase, the maximum amount of exsolution per unit volume of formation water is 0.2231~0.2351 mol/kg. Without considering the leakage of hydrocarbon gas caused by caprock sealing and diffusion during the accumulation process, the volume of circulating formation water required to generate the existing hydrocarbon gas accumulation (594.22×10^8 m^3) in the DF1-1 field is $1.13 \sim 1.19 \times 10^{13}$ kg (Table 5).

It can be seen from the above that the maximum closed area of the DF1-1 structure is 300 km^2, the depth difference between the accumulation location and the top of the source rock of the Meishan Formation is less than 2000 m, and the average porosity is 20%. The formation water capacity is

Table 5: Calculation results of formation water volume required for DF1-1 structure water soluble phase exsolution and accumulation.

Hydrocarbon gas accumulation of DF1-1	Max. exsolution	Molar volume of CH_4	Dissolvable formation water
$\times 10^8$ m^3	mol/kg	L/mol	$\times 10^{13}$ kg
594.22	0.2231~0.2351	22.36	1.13-1.19

1.19×10^{11} kg calculated by the static volume method. According to the calculation, if the structure is entirely accumulated in the form of the water-soluble phase exsolution, the formation water required is 95~100 times the maximum water capacity of the formation, which is obviously seriously inconsistent with the actual situation of the formation. It can be concluded that, for the DF1-1 structure, the hydrocarbon gas was already in the mixed phase of the water-soluble phase and free phase at the initial migration, and the free-phase migration was dominant in the accumulation process of this structure.

6. Conclusions

The solubility of CH_4 in deionized water was researched with both experimental and modeling methods. The main conclusions are shown as follows.

The solubility of CH_4 in water was measured by self-developed equipment in the temperature and pressure range of 313.15 K~473.15 K and 5 MPa~200 MPa, respectively. The empirical solubility equation of CH_4 considering the phase state of CH_4 and H_2O was established. This model is suitable for gaseous, critical, and supercritical CH_4 as well as liquid water. In the low-pressure region, the solubility mainly depends on the pressure, and the solubility value is small (usually less than 0.2 mol/kg). In the middle pressure region, the solubility mainly depends on the pressure but at a lower dependence compared to that in the low-pressure region. In the high-pressure region, the solubility was influenced by temperature more than pressure.

Based on the experimental results calculated, the maximum solubility of CH_4 in water is 0.2231~0.2351 mol/kg, and the quality of water is 1.19×10^{11} kg in DF1-1 tectonic strata. Without considering CH_4 escaped in formation, if the amount of the current CH_4 reservoir is formed by the

water-soluble phase migration, the amount of formation water required is about 100 times of the actual pore water volume in the DF1-1 structure. This is completely inconsistent with the law of geological fluid migration. Therefore, the natural gas migration and accumulation in the DF1-1 structure is the result of the interaction of the free phase and the water-soluble phase.

Data Availability

Data will be made available on request.

Conflicts of Interest

The authors declare that they have no conflicts of interest.

Acknowledgments

This topic is derived from the comprehensive scientific research project "CO_2 Accumulation Research and Risk Assessment of Key Exploration Areas in China Sea" of the Beijing Research Center of the China National Offshore Oil Corporation (Contract No.: CCL2015RCPS0162RCN).

References

[1] T. J. Xie, "Natural gas migration conducting system and reservoir formation pattern in southeast Hainan basin," *China Petroleum Exploration*, vol. 5, no. 1, pp. 17–21, 2000.

[2] J. Yuan, *Gas Accumulation Characteristics under the High Temperature and Pressure and Water-Dissolving Phase Background in the Yinggehai [D]*, China University of Petroleum-Beijing, 2009.

[3] J. Liu, Z. Huang, J. Zhu, and C. Tong, "Characteristics of water-soluble gas exsolution and accumulation in Yinggehai Basin," *Journal of China University of Petroleum (Edition of Natural Science)*, vol. 38, no. 1, pp. 32–39, 2014.

[4] C. Tong, Y. Xie, Z. Huang, and J. Ma, "Geochemical behaviors of HPHT gas reservoirs in the Yinggehai Basin and the efficient gas accumulation mode in its diapir flanks," *Natural Gas Industry*, vol. 2, no. 2-3, pp. 144–154, 2015.

[5] P. K. Frolich, E. J. Tauch, J. J. Hogan, and A. A. Peer, "Solubilities of gases in liquids at high pressure," *Industrial & Engineering Chemistry*, vol. 23, no. 5, pp. 548–550, 1931.

[6] A. Michels, J. Gerver, and A. Bijl, "The influence of pressure on the solubility of gases," *Physica*, vol. 3, no. 8, pp. 797–808, 1936.

[7] O. L. Culberson, A. B. Horn, and M. K. Jr, "Phase equilibria in hydrocarbon-water systems II - the solubility of ethane in water at pressures to 10,000 psi," *Journal of Petroleum Technology*, vol. 2, no. 11, pp. 319–322, 1950.

[8] O. L. Culberson and M. K. Jr, "Phase equilibria in hydrocarbon-water systems IV - vapor-liquid equilibrium constants in the methane-water and ethane-water systems," *Journal of Petroleum Technology*, vol. 3, no. 11, pp. 297–300, 1951.

[9] J. R. Duffy, N. O. Smith, and B. Nagy, "Solubility of natural gases in aqueous salt solutions–I," *Geochimica et Cosmochimica Acta*, vol. 24, no. 1-2, pp. 23–31, 1961.

[10] T. D. O'Sullivan and N. O. Smith, "Solubility and partial molar volume of nitrogen and methane in water and in aqueous sodium chloride from 50 to 125.deg. and 100 to 600 atm," *Journal of Physical Chemistry*, vol. 74, no. 7, pp. 1460–1466, 1970.

[11] L. C. Price, "Aqueous solubility of methane at elevated pressures and temperatures," *AAPG bulletin*, vol. 63, no. 9, pp. 1527–1533, 1979.

[12] Y. Wang, B. Han, H. Yan, and R. Liu, "Solubility of CH_4 in the mixed solvent t-butyl alcohol and water," *Thermochimica Acta*, vol. 253, no. 6, pp. 327–334, 1995.

[13] K. Y. Song, G. Feneyrou, F. Fleyfel, R. Martin, J. Lievois, and R. Kobayashi, "Solubility measurements of methane and ethane in water at and near hydrate conditions," *Fluid Phase Equilibria*, vol. 128, no. 1-2, pp. 249–259, 1997.

[14] A. Chapoy, C. Coquelet, and D. Richon, "Solubility measurement and modeling of water in the gas phase of the methane/water binary system at temperatures from 283.08 to 318.12 K and pressures up to 34.5 MPa," *Fluid Phase Equilibria*, vol. 214, no. 1, pp. 101–117, 2003.

[15] A. Chapoy, A. H. Mohammadi, D. Richon, and B. Tohidi, "Gas solubility measurement and modeling for methane–water and methane–ethane-n-butane–water systems at low temperature conditions," *Fluid Phase Equilibria*, vol. 220, no. 1, pp. 111–119, 2015.

[16] L. K. Wang, G. J. Chen, G. H. Han, X. Q. Guo, and T. M. Guo, "Experimental study on the solubility of natural gas components in water with or without hydrate inhibitor," *Fluid Phase Equilibria*, vol. 207, no. 1–2, pp. 143–154, 2003.

[17] W. Ou, L. Geng, W. Lu, H. Guo, K. Qu, and P. Mao, "Quantitative Raman spectroscopic investigation of geo-fluids high-pressure phase equilibria: Part II. Accurate determination of CH_4 solubility in water from 273 to 603 K and from 5 to 140 MPa and refining the parameters of the thermodynamic model," *Fluid Phase Equilibria*, vol. 391, pp. 18–30, 2015.

[18] Z. Duan, N. Møller, and J. H. Weare, "An equation of state for the CH_4-CO_2-H_2O system: I. Deinoized systems from 0 to 1000°C and 0 to 8000 bar," *Geochimica et Cosmochimica Acta*, vol. 56, no. 7, pp. 2605–2617, 1992.

[19] Z. Duan, N. Møller, and J. H. Weare, "An equation of state for the CH_4-CO_2-H_2O system: II. Mixtures from 50 to 1000°C and 0 to 1000 bar," *Geochimica et Cosmochimica Acta*, vol. 56, no. 7, pp. 2619–2631, 1992, to 1000°C and 0 to 1000 bar.

[20] Z. Duan and S. Mao, "A thermodynamic model for calculating methane solubility, density and gas phase composition of methane-bearing aqueous fluids from 273 to 523 K and from 1 to 2000 bar," *Geochimica et Cosmochimica Acta*, vol. 70, no. 13, pp. 3369–3386, 2006.

[21] J. Gao, D. Q. Zheng, and T. M. Guo, "Solubilities of methane, nitrogen, carbon dioxide, and a natural gas mixture in aqueous sodium bicarbonate solutions under high pressure and elevated temperature," *Journal of Chemical & Engineering Data*, vol. 42, no. 1, pp. 69–73, 1997.

[22] W. Lu, I. M. Chou, and R. C. Burruss, "Determination of methane concentrations in water in equilibrium with sI methane hydrate in the absence of a vapor phase by in situ Raman spectroscopy," *Geochimica et Cosmochimica Acta*, vol. 72, no. 2, pp. 412–422, 2008.

[23] S. Mao, Z. Duan, D. Zhang, L. Shi, Y. Chen, and J. Li, "Thermodynamic modeling of binary CH_4-H_2O fluid inclusions," *Geochimica et Cosmochimica Acta*, vol. 75, no. 20, pp. 5892–5902, 2011.

[24] H. C. Fan, Z. L. Huang, J. Yuan, G. Gao, and C. X. Tong, "Experiments on the dissolution of methane-rich natural gas and characteristics of reservoir formation by water resolution," *Journal of Jilin University (Earth Science Edition)*, vol. 41, no. 4, pp. 1033–1039, 2011.

[25] J. A. Nighswander, N. Kalogerakis, and A. K. Mehrotra, "Solubilities of carbon dioxide in water and 1 wt. % sodium chloride solution at pressures up to 10 MPa and temperatures from 80 to 200.degree.C," *Journal of Chemical & Engineering Data*, vol. 34, no. 3, pp. 355–360, 1989.

[26] H. Messabeb, F. Contamine, P. Cézac, J. P. Serin, C. Pouget, and E. C. Gaucher, "Experimental measurement of CO_2 solubility in aqueous $CaCl_2$ solution at temperature from 323.15 to 423.15 K and pressure up to 20 MPa using the conductometric titration," *Journal of Chemical & Engineering Data*, vol. 62, no. 12, pp. 4228–4234, 2017.

[27] J. Qin, R. J. Rosenbauer, and Z. Duan, "Experimental measurements of vapor–liquid equilibria of the H_2O+CO_2+CH_4 ternary system," *Journal of Chemical and Engineering Data*, vol. 53, no. 6, pp. 1246–1249, 2008.

[28] Y. Wang, P. Liu, G. Li, and S. Hu, "Formation-water characteristics and its relationship with hydrocarbon preservation, DF1-1 gasfield in Yinggehai Basin," *Natural Gas Exploration and Development*, vol. 33, no. 2, pp. 19–22, 2010.

[29] S. Zhang, B. Xia, and X. Tong, "The mid depth gas reservoir geological characters and hydrocarbon accumulation mode of DF1-1 structure in Yinggehai Basin," *Fault-block Oil & Gas Field*, vol. 6, pp. 15–18, 2004.

[30] Y. Xie and B. Huang, "Characteristics and accumulation mechanisms of the Dongfang 13-1 high temperature and overpressured gas field in the Yinggehai Basin, the South China Sea," *Science China Earth Sciences*, vol. 57, no. 11, pp. 2799–2807, 2014.

[31] X. Li, *A Study on Balance Exploitation by Optimization of Allocation Production of Dongfang Gas Field*, Xi'an Shiyou University, 2010.

[32] Z. Zeng and F. Zhou, "Mud diapiric action make contribution to forming underground thermal grounds and traps in DF1-1 gas field," *Offshore Oil*, vol. 1, pp. 24–29, 2002.

[33] R. Liu, J. Liu, W. Zhu et al., "Expulsion process of overpressure fluids indicated by vertical venting structures in the Dongfang area of the Yinggehai Basin, offshore South China Sea," *Marine and Petroleum Geology*, vol. 66, pp. 848–860, 2015.

[34] L. L. Li, "Solubility and exsolution study of CO_2 and CH_4," *China University of Geosciences (Wuhan)*, 2018.